

# Mg and Al Yields from Low and Intermediate Mass AGB stars

A. I. KARAKAS and J.C. LATTANZIO  
*Centre for Stellar & Planetary Astrophysics, Monash University, Australia*

---

## Abstract

We investigate the production of aluminium and the heavy magnesium isotopes in asymptotic giant branch (AGB) models. We evolve models with a wide range in initial mass ( $1 \geq (M_{\odot}) \geq 6$ ) and composition ( $Z = 0.02, 0.008, 0.004$ ). We evolve the models from the pre-main sequence, through all intermediate stages including the core helium flash, to near the end of the thermally-pulsing AGB phase. We then performed detailed nucleosynthesis calculations from which we determine for the first time, the production of the magnesium and aluminium isotopes as a function of the stellar mass and composition. From our models, we calculate stellar yields suitable for galactic chemical evolution models. We find that low-mass AGB stars ( $M \lesssim 3M_{\odot}$ ) do not produce the necessary temperatures to synthesize the neutron-rich magnesium isotopes in the helium shell. The most massive AGB models do produce the neutron-rich magnesium isotopes, and also produce  $^{26}\text{Al}$  in substantial quantities via hot bottom burning. We note that the calculations are subject to many uncertainties, such as the modelling of the third dredge up, mass-loss and nuclear reaction rates.

## 1.1 Introduction

In recent years our attempts to understand many aspects of nucleosynthesis and stellar evolution have come to rely on our understanding of the production of the magnesium and aluminium isotopes. For example, abundance anomalies in globular cluster stars have been a problem for many years, and the role of Mg and Al is central, and far from understood (Yong et al. 2003, Shetrone 1996). At the heart of this problem is the quest for the production site of the Mg and Al anomalies: are they produced in the star itself, and mixed to the surface by some form of deep mixing (Denissenkov & Weiss 1996) or are they the result of pollution from an earlier generation of stars? The latter would seem to implicate asymptotic giant branch (AGB) stars (Denissenkov et al 1996, Ventura et al 2001) where Mg and Al can be produced by thermal pulses and mixed into the envelope by the subsequent third dredge-up (TDU).

Although all isotopes of magnesium are produced by supernovae, low-metallicity supernovae models fail to produce enough of the neutron-rich Mg isotopes to account for the chemical evolution of  $^{25}\text{Mg}$  and  $^{26}\text{Mg}$  in the Galaxy (Gay & Lambert 2000). Other possible sources of the neutron-rich magnesium isotopes include the winds from low-metallicity Wolf-Rayet (WR) (Maeder 1983) and AGB stars (Siess et al. 2002, Forestini & Charbonnel

1997). There are currently no quantitative studies of the production of the neutron-rich Mg isotopes in low-metallicity WR stars. There are quantitative studies of magnesium production in low metallicity AGB stars (Siess et al. 2002, Forestini & Charbonnel 1997) but these studies do not cover a sufficiently large range of mass or composition to produce yields suitable for galactic chemical evolution models. For this reason, a quantitative understanding of the production of the heavy Mg isotopes in AGB models of different mass and metallicity is required if we are to understand the non-solar Mg isotopic distribution observed in various stars. For example, giants in the globular cluster NGC 6752 were observed by Yong et al. (2003) to have highly non-solar Mg isotopic ratios, with a slight excess of  $^{26}\text{Mg}$  over  $^{25}\text{Mg}$ . As the observed stars do not exhibit the luminosity variations expected if the abundance anomalies were produced internally, it was assumed that the giants were polluted by an earlier generation of stars. The authors concluded that the earlier generation of stars were likely to be a population of intermediate mass, very low metallicity ( $Z \sim 0$ ) AGB stars.

Aluminium is produced at the expense of Mg by the Mg-Al chain, a process which can produce substantial  $^{26}\text{Al}$  (Arnould et al. 1999). Whilst most of the  $^{26}\text{Al}$  observed in the Galaxy today probably originated in young massive stars (Prantzos 1993) contributions from other sources such as classical novae and low and intermediate mass AGB stars might be important (Meynet 1994). Models of classical novae by José & Hernanz (1998) find substantial  $^{26}\text{Al}$  production. The production and destruction of  $^{26}\text{Al}$  in AGB stars has been discussed in detail by Mowlavi & Meynet (1999). They found that hot bottom burning (HBB) in massive AGB stars could be an important source of  $^{26}\text{Al}$ . Nollett, Busso & Wasserburg (2003) studied parameterized extra-mixing processes in low-mass AGB models. They found that, depending on the mixing parameters used,  $^{26}\text{Al}$  can be produced in sufficient quantities to explain the amount inferred to have been present in some circumstellar oxide grains at the time of their formation. Whilst these various studies suffer from many uncertainties, they make the point that there may be many sources contributing to the  $^{26}\text{Al}$  in the Galaxy.

A quantitative study of the production of the heavy magnesium isotopes and aluminium in AGB models is the main aim of this contributed paper.

## 1.2 Stellar Models

Models were calculated with the Mount Stromlo Stellar Structure code (Wood & Zarro 1981, Frost & Lattanzio 1996) updated to include the OPAL opacities of Iglesias & Rogers (1996). Mass loss was included using the prescription of Vassiliadis & Wood (1993) but without the modification for  $M$  greater than  $2.5M_{\odot}$ . We calculated model sequences for three different initial compositions:  $Z = 0.02, 0.008$  and  $0.004$  over a range in mass  $1 \leq M_0(M_{\odot}) \leq 6$  where  $M_0$  is the initial stellar mass. Initial abundances for the CNO elements were taken from Grevesse, Noels & Sauval (1992) for the  $Z = 0.02$  models, and from Russell & Dopita (1992) for the Large Magellanic Cloud compositions ( $Z = 0.008$ ) and Small Magellanic Cloud compositions ( $Z = 0.004$ ).

We use the standard mixing-length theory for convection, with a mixing-length parameter  $\alpha = l/H_p = 1.75$ . We find the convective boundary at the base of the outer envelope by searching for a neutral border to the convective zone, in the manner described in Frost & Lattanzio (1996) and Karakas, Lattanzio & Pols (2002). We note that while this method does increase the efficiency of the TDU for low-mass models, we do not find any dredge-up for the  $Z = 0.02$  models with  $M \leq 2.0M_{\odot}$ . Reaction rates used in the evolution code were taken

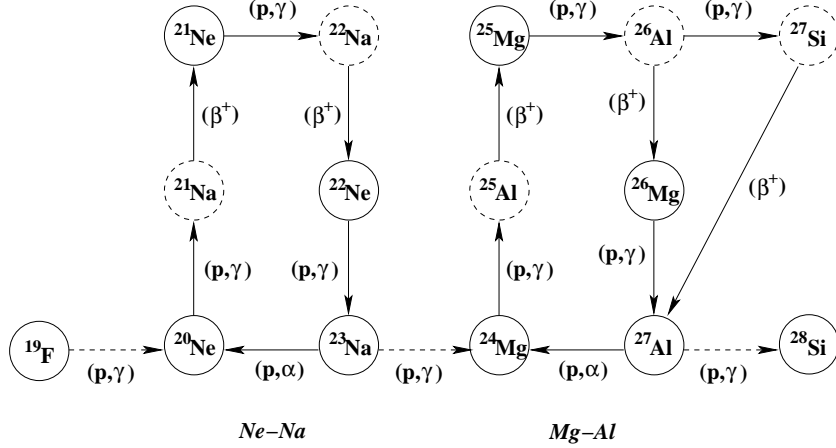


Fig. 1.1. Reactions of the Ne-Na and Mg-Al chains. Unstable isotopes are denoted by dashed circles.

mostly from Caughlan & Fowler (1988), but with updates included in the nucleosynthesis calculations (see below).

We performed detailed nucleosynthesis calculations separately using a post-processing nucleosynthesis code which includes time-dependent diffusive mixing, 506 reactions and 74 species up to sulphur. We also include a small neutron capture network based on the iron-peak elements. The bulk of the 506 reaction rates are from the Reaclib Data Tables, based on the 1991 updated version of the compilation by Thielemann, Arnould & Truran (1991). We include recent reaction rates for  $\alpha$ , proton and neutron capture reactions when available, as detailed in Lugaro (1998).

### 1.3 Production of Mg and Al in AGB stars

The magnesium and aluminium isotopes are produced in three sites in AGB stars: the hydrogen-burning shell (H-shell) via the Mg-Al chain, shown in Fig. 1.1 (Rolfs & Rodney 1988); the helium-burning shell (He-shell) via  $\alpha$ -capture on  $^{22}\text{Ne}$  and at the base of the convective envelope in the most massive AGB stars that experience HBB, again via the Mg-Al chain. The efficiency of production of each site depends in a complicated way on the temperature (i.e. via the initial mass), initial composition and the extent to which each site affects the other.

#### 1.3.1 Hydrogen-burning shell

Magnesium and aluminium are produced in the H-burning shell via the activation of the Mg-Al chain. In Fig. 1.1 we show the reactions involved in the Ne-Na and the Mg-Al chains (Arnould et al. 1999, Rolfs & Rodney 1988). The first isotope in the Mg-Al chain to be affected is  $^{25}\text{Mg}$ , which is burnt to  $^{26}\text{Al}$  when the temperature exceeds about 30 million K. The isotope  $^{26}\text{Al}$  is unstable to  $\beta$ -decay but the lifetime of  $\beta$ -decay relative to proton capture generally favours proton capture within the H-burning shell. This produces the unstable  $^{27}\text{Si}$  which  $\beta$ -decays (with a lifetime on the order of a few seconds) to  $^{27}\text{Al}$ . If temperatures exceed 70 million K,  $^{24}\text{Mg} + \text{p}$  leads to the production of  $^{25}\text{Mg}$  along with  $^{26}\text{Al}$  and  $^{27}\text{Al}$ .

In low-mass models\*, the only change to the surface abundance of the Mg and Al isotopes comes from the H-burning shell. The ashes of the H-burning shell are first engulfed by the convective pocket before dredge-up occurs. In low-mass models, the Mg isotopes are not effected by He-shell burning but  $^{26}\text{Al}$  can be destroyed by neutron capture. Neutrons come from two reactions in AGB stars:  $^{13}\text{C}(\alpha, n)^{16}\text{O}$  and  $^{22}\text{Ne}(\alpha, n)^{25}\text{Mg}$ . As the temperature is too low for the activation of the  $^{22}\text{Ne}$  neutron source, the only free neutrons are from the  $^{13}\text{C}$  neutron source. We do not include a  $^{13}\text{C}$  pocket in our models, so the neutrons in the convective pocket are from the  $^{13}\text{C}$  left by the H-burning shell.

We find that the change to the envelope composition in low-mass models with efficient TDU is a slight depletion of  $^{25}\text{Mg}$  and a slight increase in the abundance of  $^{26}\text{Mg}$  and  $^{27}\text{Al}$ . The  $^{24}\text{Mg}$  abundance remained unchanged. Owing to the lack of an efficient neutron source in the low-mass models, we find that the surface abundance of  $^{26}\text{Al}$  slowly increases with each dredge-up episode. By the end of the TP-AGB phase, the  $^{26}\text{Al}/^{27}\text{Al}$  ratio could be as high as  $\text{few} \times 10^{-3}$  at the surface; except for the  $Z = 0.02$  models, where we find this ratio to be about 100 times smaller. We demonstrate the effect of H-burning nucleosynthesis in Fig. 1.2. In the top panel of Fig. 1.2 we plot the composition profile of the  $1.5M_{\odot}$ ,  $Z = 0.004$  model just before the 14<sup>th</sup> thermal pulse, showing the He- and H-burning shells. The shaded region denotes the convective envelope. The maximum extent of the convective pocket during the 14<sup>th</sup> thermal pulse is noted. In the lower panel of Fig. 1.2 we plot the composition profile at the maximum extent of the TDU, after the pulse. The composition of  $^{26}\text{Al}$  in the intershell has been homogenized by the convective pocket, but is not destroyed from neutron capture. We find that after dredge up occurs, the surface abundance of  $^{26}\text{Al}$  has increased by about 30%.

In conclusion, the operation of the H-shell in low-mass models is quantitatively unimportant to the production of the Mg isotopes. Some  $^{26}\text{Al}$  could be produced in low-mass, low-metallicity AGB models, but this conclusion suffers from many uncertainties. As we discuss in the next two sections, the operation of the He-burning shell and HBB is much more important in intermediate and massive AGB models than the H-burning shell.

### **1.3.2 Helium-burning shell**

The He-burning shell in AGB stars is a rich source of nucleosynthesis. The main result is the production of  $^{12}\text{C}$ , which when mixed to the surface may produce carbon stars. There is also a wealth of other He-burning products such as  $^{22}\text{Ne}$ ,  $^{25}\text{Mg}$ ,  $^{26}\text{Mg}$  (Forestini & Charbonnel 1997) and s-process elements (Busso et al. 2001).

Substantial  $^{22}\text{Ne}$  is created during a thermal pulse by  $\alpha$ -capture onto the  $^{14}\text{N}$  left by the H-burning shell during the preceding interpulse period. If the temperature exceeds about 300 million K, then  $^{25}\text{Mg}$  and  $^{26}\text{Mg}$  can be produced in substantial quantities by  $\alpha$ -capture onto  $^{22}\text{Ne}$  via the reactions  $^{22}\text{Ne}(\alpha, n)^{25}\text{Mg}$  and  $^{22}\text{Ne}(\alpha, \gamma)^{26}\text{Mg}$ . In Fig. 1.3 we plot the time variation of the intershell abundances of  $^{22}\text{Ne}$ ,  $^{25}\text{Mg}$  and  $^{26}\text{Mg}$  for the  $4M_{\odot}$ ,  $Z = 0.008$  model. We plot the abundances in the intershell convective region for the 15<sup>th</sup> to the 20<sup>th</sup> thermal pulse. The abundance for each species initially decreases due to the growth of the convective shell into the region previously processed by the H-shell. At the end of the preceding interpulse phase this region has been depleted in  $^{22}\text{Ne}$ ,  $^{25}\text{Mg}$  and  $^{26}\text{Mg}$  via H burning. As the temperature in the intershell convective region increases, successive  $\alpha$ -

\* hereafter low-mass refers to models with  $M \leq 2.5M_{\odot}$

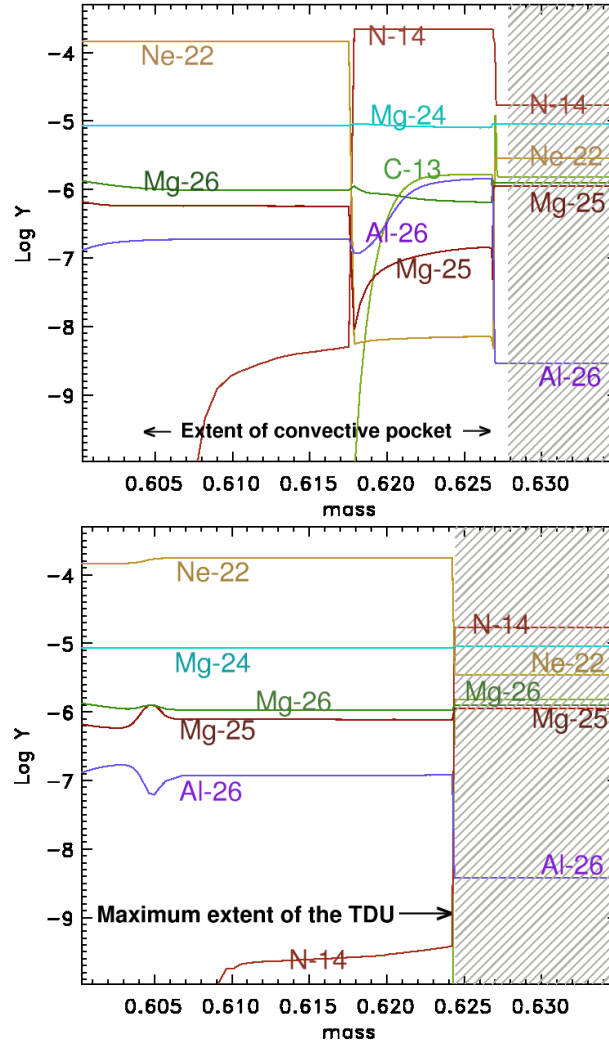


Fig. 1.2. Composition profile for the  $1.5M_{\odot}$ ,  $Z = 0.004$  model just before the 14<sup>th</sup> thermal pulse (top panel) and at the maximum extent of the following dredge up episode (lower panel).

captures onto  $^{14}\text{N}$  first produces an increase in the  $^{22}\text{Ne}$  abundance followed by an increase in  $^{25}\text{Mg}$  and  $^{26}\text{Mg}$  when the temperature reaches exceeds 300 million K. Note that after the intershell convective pulse dies down, the final  $^{22}\text{Ne}$  abundance is still high, making it the third most abundant species in this region (after He and  $^{12}\text{C}$ , but higher than  $^{16}\text{O}$ ).

The exact amounts of  $^{25}\text{Mg}$  and  $^{26}\text{Mg}$  produced in the He-shell is dependent not only on the reaction rates but also on the abundance of matter left by the H-burning shell. As the ashes of the H-shell are engulfed by the next thermal pulse, the initial abundances of the two heavy magnesium isotopes can be quite different. For example, in the  $6M_{\odot}$ ,  $Z = 0.004$  model, we find that the abundance of  $^{25}\text{Mg}/^{26}\text{Mg}$  can be as low as 0.2 at the beginning of a

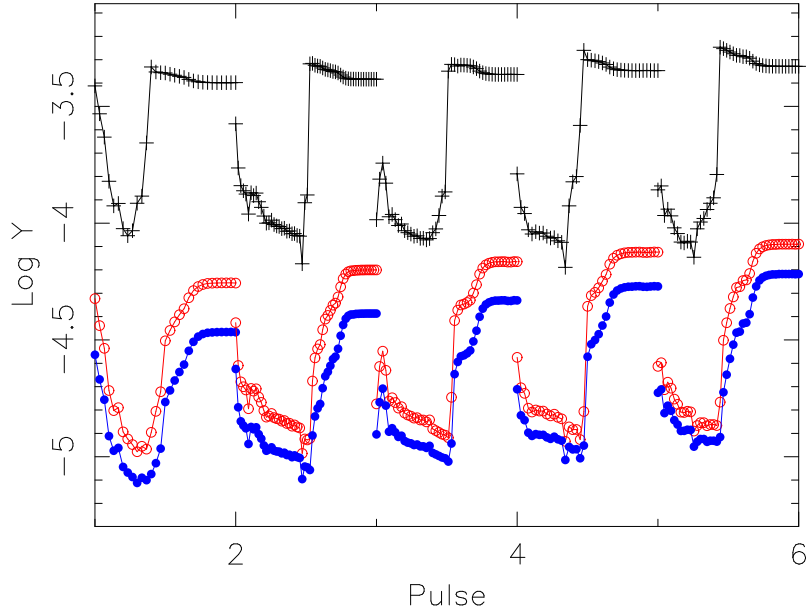


Fig. 1.3. The intershell abundances of  $^{22}\text{Ne}$  (black plus signs),  $^{25}\text{Mg}$  (red open circles) and  $^{26}\text{Mg}$  (blue closed circles) as a function of pulse number. In this diagram we plot the intershell abundances for the 15th to the 20th pulse, but only during the time when the convective shell is present; the x-axis is the (scaled) duration of the convective pocket. Note that the abundances are the logarithm of the mole fraction,  $Y$ .

thermal pulse (c.f. the initial ratio  $^{25}\text{Mg}/^{26}\text{Mg} \sim 0.9$ ). For this model, even if the temperature in the He-shell favours the production of  $^{25}\text{Mg}$  over  $^{26}\text{Mg}$ , we still find  $^{25}\text{Mg}/^{26}\text{Mg} \sim 0.65$  at the end of the thermal pulse (prior to TDU).

We find temperatures exceed 300 million K in the He-shells of models with  $M \gtrsim 3M_{\odot}$ , depending on the initial composition. However we only find substantial  $^{25}\text{Mg}$  and  $^{26}\text{Mg}$  production in the most massive AGB models. Thus we can conclude that the He-burning shell is the most efficient production site of the neutron-rich Mg isotopes in AGB stars but only in the most massive AGB models.

### 1.3.3 Hot-bottom burning

If the temperature at the base of the convective envelope reaches about 60 million degrees K, *hot bottom burning* can occur, which is to say that the bottom of the convective envelope reaches into the top of the H-burning shell. We find H-burning primarily through the CNO cycle but also the Ne-Na and Mg-Al chains if the temperature is high enough. This site then becomes important for the production of many elements, including primary nitrogen (Chieffi et al. 2001), lithium (Travaglio et al 2001) and sodium (Mowlavi 1999).

At the base of the convective envelope, the Mg-Al chain follows the same sequence as seen in the H-shell. We note that although the region hot enough for H-burning is quite thin, owing to efficient mixing the entire envelope passes through the hot region at least 1000 times per interpulse. In Fig. 1.4 we plot the time variation of some species at the surface of

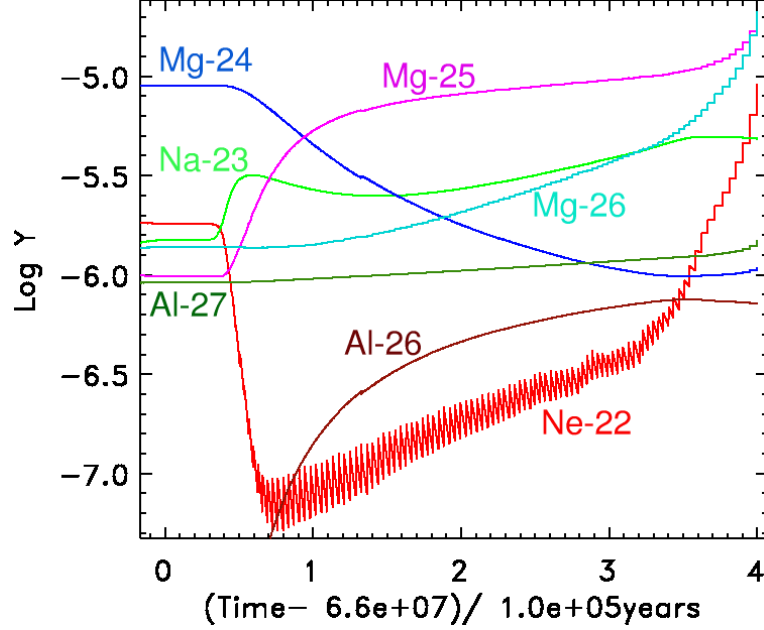


Fig. 1.4. Surface abundance evolution during the AGB of the neon, sodium and magnesium isotopes for the the  $6M_{\odot}$ ,  $Z = 0.004$  model.

the  $6M_{\odot}$ ,  $Z = 0.004$  model. This figure demonstrates the most extreme behaviour we found in the HBB models, with temperatures exceeding 94 million K at the base of the convective envelope. We find large depletions in  $^{24}\text{Mg}$  and  $^{22}\text{Ne}$  followed by significant enhancements in  $^{25}\text{Mg}$ ,  $^{26}\text{Mg}$  and  $^{26}\text{Al}$ . We also find moderate enhancements in  $^{23}\text{Na}$  and  $^{27}\text{Al}$ . This model was also significantly depleted in  $^{16}\text{O}$  via HBB. After mass loss reduced the mass of the envelope below about  $2M_{\odot}$ , the temperature was too low for HBB and the continuation of dredge-up turned the model into an obscured carbon star, with  $\text{C/O} \geq 1$  (see Frost et al 1998).

We conclude the HBB can be an efficient production site for  $^{26}\text{Al}$  and  $^{27}\text{Mg}$  at the expense of the Mg isotopes. We note the most abundant isotope,  $^{24}\text{Mg}$  is not burnt via HBB unless the temperature at the base of the envelope exceeds about 80 million K.

#### 1.4 Results and Discussion

We calculate stellar yields according to the following definition:

$$M_k = \int_0^{\tau} [X(k) - X_0(k)] \frac{dM}{dt} dt, \quad (1.1)$$

where  $M_k$  is the *net* yield of species  $k$  (in solar masses),  $dM/dt$  is the current mass-loss rate,  $X(k)$  and  $X_0(k)$  refer to the current and initial mass-fraction of species  $k$  and  $\tau$  is the total lifetime of the stellar model. The net yield can be negative, in the case where the element is destroyed in the star and the final value is lower than that during the main-sequence phase. A positive net yield corresponds to those elements produced in the star so there is a net enrichment over the stellar lifetime at the surface.

In practice, our models does not lose the entire envelope during the TP-AGB evolution owing to convergence difficulties near the end of the AGB phase. For the lower masses considered, the remaining envelope mass is very small, and is certainly less than will be lost during the subsequent interpulse phase. In these cases we calculate the yield by simply removing the small remaining envelope with its current composition. For the more massive models considered, there may be enough envelope mass remaining for a few more thermal pulses to occur. HBB has been terminated, however, so the species most affected are those which are present in the intershell convective zone. To calculate the stellar yields in these cases we will use the principles of synthetic AGB evolution to calculate the enrichment from the few remaining thermal pulses. We do not go into details of the synthetic model but refer the reader to Karakas & Lattanzio (2003).

In Fig. 1.5 we plot the yields of  $^{25}\text{Mg}$  (upper panel),  $^{26}\text{Mg}$  (middle panel) and  $^{26}\text{Al}$  (lower panel) as a function of the stellar mass and composition. We weight the stellar yields by the initial mass function of Kroupa, Tout & Gilmore (1993). In each figure, the black solid line (and points) refer to the  $Z = 0.02$  models, the blue dashed line (and open squares) refer to the  $Z = 0.008$  models and the red dot-dashed line (and open circles) refer to the  $Z = 0.004$  models. We plot for comparison the yields of Forestini & Charbonnel (1997) (hereafter FC97), also weighted by the IMF. The solid green squares are the  $Z = 0.02$  results from FC97 and the solid magenta triangles the  $Z = 0.005$  results from FC97. The first thing we note from Fig. 1.5 is that the yields are highly metallicity dependent. For the three species considered, the  $Z = 0.004$  yields are considerably larger than the  $Z = 0.02$  yields. The yields are also highly dependent on the initial stellar mass. As expected, low-mass models contribute little to the production of neutron-rich Mg isotopes,  $^{25}\text{Mg}$  and  $^{26}\text{Mg}$  or to the radionuclide  $^{26}\text{Al}$ . Also as expected from the above discussion, the yields from the models with HBB produce the largest amount of  $^{26}\text{Al}$ . If we compare our results to FC97 we find we produce more of the neutron-rich Mg isotopes at all masses and metallicities. We also produce more  $^{26}\text{Al}$  in the  $Z = 0.008$  and  $Z = 0.004$  models but about the same at  $Z = 0.02$ .

The large difference between our yields and those of FC97 is most likely explained by the different modelling approaches used. We used detailed stellar models for most of the TP-AGB phase, only resorting to synthetic modelling for the final few thermal pulses. This means that we do not have to treat HBB synthetically, as HBB had ended by the time the detailed model calculations ceased. In comparison, FC97 use detailed modelling for the pre-AGB phase and a few thermal pulses. The majority of the thermal pulses, and the HBB phase, were calculated synthetically. The surface abundance changes caused by HBB are highly dependent on the temperature (and the density) at the base of the convective envelope. If these quantities are not treated correctly in the synthetic model, the resulting yields will be quite different to those found from detailed modelling. For example, FC97 extrapolated the behaviour of the temperature at the base of the envelope forward in time, realising that this extrapolation was likely to be incorrect. The differences between synthetic and detailed modelling also applies to those species affected by He-shell burning, such as the neutron-rich Mg isotopes. A synthetic calculation can not follow the change to the intershell composition with time. Indeed, most calculations (Marigo 2001) assume that the intershell composition remains constant over the entire TP-AGB phase. We find that the intershell abundance varies not only with mass but also with time, and that the peak production of some species is found right at the end of the TP-AGB, when the He-shell is hottest.



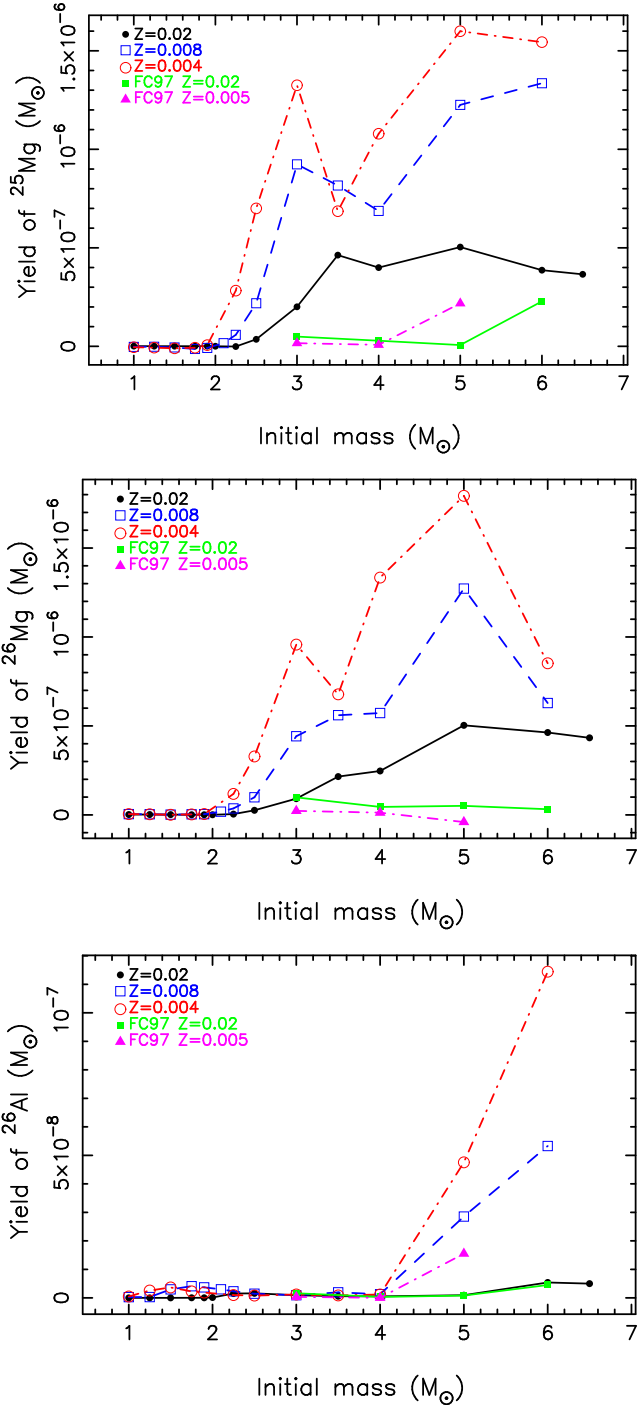


Fig. 1.5. Weighted yield of  $^{25}\text{Mg}$  (upper panel),  $^{26}\text{Mg}$  (middle) and  $^{26}\text{Al}$  (lower panel) as a function of the initial stellar mass (in  $M_{\odot}$ ). See text for a description of the symbols.

We also note that the stellar yields are also dependent on the final remnant mass. The final mass of a stellar model depends on the details of the previous core H and He-burning phases as well as on the mass-loss rates. These details can differ dramatically from one calculation to another, making direct comparison difficult.

## 1.5 Conclusions

In conclusion, we find that intermediate mass TP-AGB models can produce substantial quantities of the neutron-rich Mg isotopes from He-shell burning. The most massive AGB models can also produce substantial  $^{26}\text{Al}$  from HBB. The yields presented here are subject to many uncertainties, including the modelling of the third dredge up as well as reaction rate uncertainties. Recent observations of non-solar Mg isotopic ratios could help constrain some of these uncertainties. For example, Yong et al. (2003) found non-solar Mg isotopic ratios in giant stars in the globular cluster stars NGC 6752, with a slight excess of  $^{26}\text{Mg}$  over  $^{25}\text{Mg}$  in most of the stars. Yong et al. (2003) discuss the possibility of AGB stars polluting the stars in this cluster. Whilst our more massive models ( $\sim 5M_{\odot}$ ) produce Mg isotopic ratios consistent with their observations, most of our models have an excess of  $^{25}\text{Mg}$  over  $^{26}\text{Mg}$ . Clearly further work needs to be done, including low-metallicity AGB models and a detailed study of the dependence of mass-loss and the reaction rate uncertainties on the yields.

## References

- Arnould, M., Goriely, S. & Jorissen, A. 1999, *A&A*, 347, 572  
Busso, M., Gallino, R., Lambert, D. L., Travaglio, C. & Smith, V. V. 2001, *ApJ*, 557, 802  
Denissenkov, P. A. & Weiss, A. 1996, *A&A*, 308, 773  
Denissenkov, P. A., Da Costa, G. S., Norris, J. E. & Weiss, A. 1998, *A&A*, 333, 926  
Caughlan, G. R. & Fowler, W. A. 1988, *Atom. Data Data Tables*, 40, 283  
Chieffi, A., Domínguez, I., Limongi, M. & Straniero, O. 2001, *ApJ*, 554, 1159  
Forestini, M. & Charbonnel, C. 1997, *A&AS*, 123, 241  
Frost, C. A., Cannon, R. C., Lattanzio, J. C., Wood, P. R. & Forestini, M. 1998, *A&A*, 332, L17  
Frost, C. A. & Lattanzio, J. C. 1996, *ApJ*, 344, L25  
Gay, P. L. & Lambert, D. L. 2000, *ApJ*, 533, 260  
Grevesse, N., Noels, A., Sauval, A. J. 1992, in *Proc. of the First SOHO Workshop: Coronal Streams, Coronal Loops, and Coronal and Solar Wind Composition*, 305  
Iglesias, C. A. & Rogers, F. J. 1996, *ApJ*, 464, 943  
José, J. & Hernanz, M. 1998, *ApJ*, 494, 680  
Karakas, A. I. & Lattanzio, J. C. 2003, *PASA*, submitted  
Karakas, A. I., Lattanzio, J. C. & Pols, O. R. 2002, *PASA*, 19, 515  
Kroupa, P., Tout, C. A. & Gilmore, G. 1993 *MNRAS*, 262, 545  
Lugaro, M. A. 1998, in *Proc. of the Fifth International Symposium on Nuclei in the Cosmos*, eds. N. Prantzos & S. Harissopulos (Editions Frontières, France), 501  
Maeder, A. 1983, *A&A*, 120, 113  
Marigo, P. 2001, *A&A*, 370, 194  
Meynet, G. 1994, *ApJS*, 92, 441  
Mowlavi, N. 1999, *A&A*, 350, 73  
Mowlavi, N. & Meynet, G. 2000, *A&A*, 361, 959  
Nollett, K. M., Busso, M. & Wasserburg, G. J. 2003, *ApJ*, 582, 1036  
Prantzos, N. 1993, *ApJ*, 405, L55  
Rofls, C. E. & Rodney, W. S. 1988, in *Cauldrons in the Cosmos*, (University of Chicago Press)  
Russell, S. C. & Dopita, M. A. 1992, *ApJ*, 384, 508  
Shetrone, M. D. 1996, *AJ*, 112, 2639

*A. I. Karakas and J.C. Lattanzio*

- Siess, L., Livio, M. & Lattanzio, J. C. 2002, ApJ, 570, 329  
Thielemann, F.-K., Arnould, M. & Truran, J. W. 1991, in Advances of Nuclear Astrophysics, eds.  
E. Vangioni-Flam et al. (Editions Frontières), 525  
Travaglio, C., Randich, S., Galli, D., Lattanzio, J. C., Elliott, L. M., Forestini, M., & Ferrini, F. 2001, ApJ, 559, 909  
Wood, P. R. & Zarro, D. M. 1981, ApJ, 248, 311  
Vassiliadis, E. & Wood, P. R. 1993, ApJ, 413, 641  
Ventura, P., D'Antona, F., Mazzitelli, I. & Gratton, R. 2001, ApJ, 550, L65  
Yong, D., Grundahl, F., Lambert, D. L., Nissen, P. E. & Shetrone, M. D. 2003, A&A, accepted